Vulnerability and Hardening Studies of Optical and Illumination Systems at MGy Dose Levels

T. Allanche, P. Paillet, V. Goiffon, C. Muller, M. van Uffelen, L. Mont-Casellas, O. Duhamel, C. Marcandella, S. Rizzolo, P. Magnan, et al.

Vulnerability and Hardening Studies of Optical and Illumination Systems at MGy Dose Levels

T. Allanche, *Student Member, IEEE*, P. Paillet, *Senior Member, IEEE*, V. Goiffon, *Member, IEEE*, C. Muller, M. Van Uffelen, *Senior Member, IEEE*, L. Mont-Casellas, O. Duhamel, C. Marcandella, S. Rizzolo, *Member, IEEE*, P. Magnan, R. Clerc, T. Lépine, M. Hébert, A. Boukenter, Y. Ouerdane, R. Scott, W. De Cock, and S. Girard, *Senior Member, IEEE*

***Abstract*— In the framework of the fusion for energy radiation hard imaging system project, the main radiation effects affecting the image quality of a miniaturized complementary metal–oxide–semiconductor-based camera exposed to radiation doses up to 1 MGy(SiO_2) are investigated for ITER applications. The radiation effects related to two of the three subcomponents of the camera are investigated: the optical system (OS) and the illumination system (IS). Subsystem demonstrators have been manufactured selecting radiation tolerant or hardened materials and components to demonstrate the feasibility to withstand such high dose levels while fulfilling the ITER remote handling needs in terms of optical performances and miniaturization. Regarding the OS, the observed degradation of the radiation-hardened optical glasses used for the OS lenses is characterized in terms of both radiation-induced attenuation and radiation-induced refractive-index change. At the system level, impact of these phenomena on the OS demonstrator performances is discussed in terms of image contrast. Radiation test results highlight the high radiation tolerance of manufactured monochrome and color OS to both degradation mechanisms. Regarding the IS, the selected architecture consists in a ring of 20 commercially available light-emitting diodes (LEDs) with monochrome (amber) or white emissions. An appropriate choice for the LEDs allows designing an IS with the requested performances and slight degradation of its output power at the MGy dose levels. From the obtained results, developing miniaturized IS and OS subcomponents for MGy dose operation levels appears realistic using commercially available technologies and appropriate hardening procedures.**

***Index Terms*— Gamma rays, light-emitting diodes (LEDs), optical materials, optical systems (OS), radiation effects.**

T. Allanche, R. Clerc, T. Lépine, M. Hébert, A. Boukenter, Y. Ouerdane, and S. Girard are with the Laboratory Hubert Curien, UMR-CNRS 5516, Université de Saint-Etienne, F-42000 Saint-Etienne, France (e-mail: t.allanche@univ-st-etienne.fr; sylvain.girard@univ-st-etienne.fr).

P. Paillet, O. Duhamel, and C. Marcandella are with CEA, DAM, DIF, F-91297 Arpajon, France.

V. Goiffon, S. Rizzolo, and P. Magnan are with ISAE-SUPAERO, Université de Toulouse, F-31055 Toulouse, France.

C. Muller is with the Laboratory Hubert Curien, UMR-CNRS 5516, Université de Saint-Etienne, F-42000 Saint-Etienne, France, and also with CEA, DAM, DIF, F-91297 Arpajon, France.

M. Van Uffelen and L. Mont-Casellas are with Fusion For Energy, 08019 Barcelona, Spain.

R. Scott is with Oxford Technologies, Abingdon OX14 1RL, U.K.

W. De Cock is with SCK-CEN, 2400 Mol, Belgium.

Digital Object Identifier 10.1109/TNS.2017.2783187

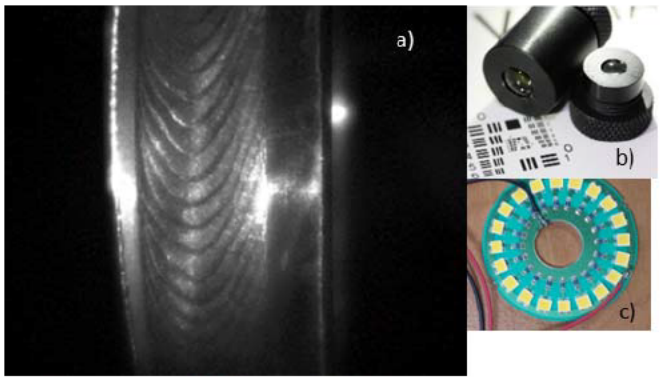

Fig. 1. (a) 600 nm monochromatic picture of a representative ITER welded steel ring. (b) FURHIS developed OS color (left) and monochrome (right). (c) Developed FURHIS IS architecture.

I. Introduction

ITER project aims to build a fusion device with the goal of demonstrating the scientific and technical feasibility of the fusion power [1]. One of the numerous encountered challenges concerns the development of radiation-hardened vision systems (mono or polychromatic) to support the remote handling operations such as pipe weld inspections in the most radiation exposed areas of the facility. Fig. 1(a) represents a typical scene of interest for one of the ITER welding inspection applications. Today, none of the commercial off-the-shelf (COTS) cameras can respond to the worst case ITER needs in terms of radiation resistance (up to a few MGy level) and also small volume (small-size camera) allowing their integration in the various inspection tools [2].

Our study, as [3], takes place in the framework of the fusion for energy (F4E) radiation hard imaging system (FURHIS) project funded by F4E, the European agency responsible for Europe's contribution to ITER. FURHIS main objective is to demonstrate that radiation-hardened miniaturized subcomponents of monochrome and color cameras can be developed achieving excellent optical performances while operating at MGy dose levels.

In this paper, the main FURHIS results are presented. First, we detail the selected procedure to evaluate the photometry budget of the camera for the targeted remote handling application and then define the architectures of the two subsystems allowing to meet the optical needs. We focus here on the optical system (OS) and illumination system (IS), whereas

the complementary radiation-hardened complementary metal–oxide–semiconductor image sensor (CIS) is addressed in [3]. Hardening the various subsystems at the component level appears mandatory to overcome the existing limitations that are reached at doses of 100 kGy for COTS camera based on CIS technologies [2]. The hardening of each component as well as the hardening of the camera at the system level will be both considered in this paper.

II. ITER Needs/Experimental Procedure

The following application functional requirements for the camera have been considered:

1) *allowed volume*: $40 \times 40 \times 76$ mm^3;
2) *temperature range*: from room temperature (RT) to 70 °C;
3) *scene definition*: working distance of 100 mm and scene size of 20×20 mm^2;
4) *radiation levels*: up to 1 MGy(SiO_2) of γ-rays.

The most promising technologies for the OS and IS have been identified from literature survey and consortium backgrounds. Based on these application input parameters, knowing the main properties of the CIS (pixel size, number, and quantum efficiency) and fixing some OS characteristics such as its aperture (F/5), the whole photometry budget can then be calculated, considering also the nature of the weld object and its optical properties with respect to the illumination source (either monochromatic or polychromatic). From the outcome of these calculations, we were able to define the possible IS architectures respecting the allowed volume and being efficient in terms of thermal management. Several demonstrators were manufactured for the OS and IS (see Fig. 1(b) and (c)) with the most promising technologies in terms of radiation hardness allowing to fulfill the ITER needs for image resolution and camera size. In parallel, different technologies for components and materials have been tested to identify the most promising off-the-shelve technologies. Light-emitting diodes (LEDs) technology has been selected for the IS and our survey of available LED technologies reveals large differences in their radiation responses. For the OS, while it is obvious that the glass darkening by radiation (leading to a degradation of the glass transmission) has to be minimized, to our knowledge no spectral radiation-induced attenuation (RIA) data exist at such dose levels. Furthermore, radiation-induced refractive-index change (RIRIC) that is identified as a major risk is almost not documented in the literature, except for space-related applications [4] limited to doses up to 4 kGy.

A. Illumination System

Radiation effects on LED performances are well documented [5] but mostly for low-dose space applications (except [6], see later). Furthermore, as atom displacement damages are mainly responsible for LED degradations [7], these studies mostly focused on proton irradiation rather than γ-rays. In a 2013 review paper [5], only two previous papers published in 2002 and 2005 dealing with γ-ray effects on visible emitting diodes were discussed. The first one [8] focuses on the electrical characterization of n-GaN LEDs irradiated up to 0.21 MGy. The second one [6] discusses the degradation of the optical output power of InGaN/GaN LEDs in the range between 410 and 510 nm up to 20 MGy. Since 2013, two other studies have been published [9], [10]. First one [9] investigates the response of 590 nm AlGaInP LEDs up to 0.3 MGy, whereas the second one [10] considers visible red LEDs for telecommunication applications. LEDs characteristics and measured optical power changes reported in these previous studies are summarized in Table I.

TABLE I
Main Characteristics of Gamma Irradiated LEDs in the Literature and Evolution in Terms of Optical Power

Ref	Type	spectral range (nm)	Max radiation level	change %	year	Silicon lens
[6]	InGaN	410 to 510	2 MGy	80	2005	w/o
[9]	AlGaInP	590	0.3 MGy	35	2013	?
[10]	AlGaInP	575	1 MGy	90	2016	with
	AlGaInP	609	1 MGy	80	2016	with
	AlGaInP	635	1 MGy	40	2016	with

Here, we complete this state of the art by performing a comprehensive survey of the response of various technologies of COTS LEDS up to MGy dose of γ-rays. Two main classes of LEDs are investigated; their details are given in Table II, amber LEDs for monochromatic (∼600 nm) cameras and white LEDs for color cameras. While most of the white LED is based on a blue emission provided by an InGaN LED and a down conversion by phosphors, two different technologies co-exist for amber LEDs: direct emission AlInGaP device, and blue InGaN LED with phosphor conversion [11].

For two of the references (A#3 and W#5), two versions of the same LEDs have been tested: one with its silicone lens and the other without it (removed by mechanical process). The silicon lens optimizes the angular distribution of the light emitted by the diode but was expected to degrade the LED radiation resistance through its radiation-induced darkening.

B. Optical System

Considering the ITER harsh environment, the main radiation effects to mitigate for the OS are the RIA and the RIRIC, whereas radiation-induced emission is expected to be negligible at the considered dose rates. From previous results obtained by space agencies, it is expected that most of the COTS bulk glasses present too strong RIA to be considered for our application [12]. If the OS were designed with such glasses, the lens degradation will be so high that the camera functionality will not be maintained even if the CIS and IS are radiation hardened. A limited number of Rad–Hard (RH) glasses are available from the manufacturer SCHOTT Ltd. [13]. They are rated as RH regarding their reduced darkening at dose levels associated with space applications and above. They are typically obtained by adding Cerium (Ce) into the glass allowing to reduce its RIA in the visible domain [14]. The drawback of this co-doping is an increased intrinsic glass attenuation below 500 nm. Only a few data are available regarding the radiation responses of these glasses at the MGy level [13] and only a very few data at low dose about

TABLE II
MAIN CHARACTERISTICS OF TESTED LEDS

Ref.	Type	Techno.	Silicon Lens	Current (mA)	Voltage (V)	Lum. Flux (lm)
A#1	Amber	AlInGaP	w/o	150	3.2	26.8
A#2	Amber	AlInGaP	/	350	3.2/3.6	48/86
A#3	Amber	InGaN Phosphor-Converted	With & w/o	350	2.8	110
W#1	White	InGaN	with	350	11.3	510
W#2	White	InGaN	w/o	150	3.2	40
W#3	White	InGaN	w/o	150	3.4	48
W#4	White	InGaN	w/o	350/700	3.2	100/170
W#5	White	InGaN	with & w/o	350/700	3.2-3.6	130/222
W#6	White	Not known	w/o	500	2.8	125

RIRIC effects [4]. An important outcome of these previous studies is that the amplitudes of the RIA and RIRIC are not correlated, i.e., an RH glass can be very sensitive to RIRIC, as the LaK9G15 glass [4] or not. RIRIC is then a major risk for RH camera for systems designed without motorized zoom, as it will directly impact the image resolution, acting as a defocusing of the OS. Five glasses have been selected for this paper:

1) *three RH glasses from SCHOTT Ltd*: BK7G18 (crown), K5G20 (crown), and SF6G06 (flint);
2) *SUPRASIL* (crown) an UV grade pure silica;
3) *BK7* (crown) as reference of a non-RH glass.

If only one glass type can be used for the design of a monochromatic OS, designing a color-one implies to combine lenses done in several glasses (crown, flint) to compensate their natural chromatic dispersions.

C. Irradiation Conditions

γ-ray tests were performed at the ^{60}Co source in the Brigitte underwater-γ-irradiation-facility at SCK-CEN (Mol, Belgium) [16]. Three consecutive runs have been performed to accumulate doses of 0.1, 0.4, and 0.6 MGy, providing data on LEDs and glasses irradiated at 0.1, 0.5, and 1.1 MGy.

D. Sample Characterizations

Bulk Samples—All measurements (RIA, RIRIC) have been performed at Laboratoire Hubert Curien (France), before and after irradiation providing information only on the damages permanent at RT. RIA spectral dependence was measured with a LAMBDA 900 spectrometer from PerkinElmer in the 300 to 850 nm range. RIRIC measurements were performed with an Abbemat Anton-Paar Ltd refractometer allowing to characterize the glass refractive indexes at eight different wavelengths in the visible domain.

LEDs Samples—For the characterization of the radiation effects on LEDs, their emission properties were measured before and after γ-ray exposure with a Labsphere Ltd LCS-100 system consisting in an integrating sphere, a calibration lamp, and a spectrometer. This test bench measures the absolute value of the LED emitted power F_T in W/nm between 300 and 800 nm. The calibration lamp allows determining the conversion factors $R_S(\lambda)$ between the spectrometer's counts and the light power (W) through

$$R_s(\lambda) = \frac{F_e(\lambda)}{S_e(\lambda)} \tag{1}$$

where $F_e(\lambda)$ is the spectral radiant flux of the calibration lamp in W/nm certified by the manufacturer and $S_e(\lambda)$ in spectrometer signal in count/nm. The total power F_T in W/nm of the tested LED is then

$$F_T = \sum_{\lambda=0}^{+\infty} R_S(\lambda) * (S_{\mathrm{LED}}(\lambda) - B(\lambda)) \tag{2}$$

where S_{LED} is the measured LED spectrum and $B(\lambda)$ the setup noise, both in count/nm. Each LED was irradiated unbiased but characterized at its nominal voltage before and after the irradiation.

Welding Samples—Two types of measurements were used to characterize the optical properties of the ITER welded steel ring. The first one is a goniophotometer REFLET by STIL Ltd allowing to measure the bidirectional reflectance distribution function [17] and a Cary-5000 by AGILENT Ltd equipped with an integrating sphere to evaluate its reflection properties.

OS Samples—Two different OS have been manufactured in the framework of FURHIS: a monochromatic OS and a polychromatic OS. In this paper, we focus on the characterization of the monochromatic one. Our criterion to evaluate the quality of the OS is the contrast C

$$C = \frac{E_{\max} - E_{\min}}{E_{\max} + E_{\min}} < 1 \tag{3}$$

where E is the irradiance in $W \cdot m^{-2}$. The contrast gives an information about the smallest detail the OS can resolve for given the IS, scene, and CIS. This contrast will be strongly affected by RIRIC; even it clearly appears that the amplitude of RIRIC impact will also depend on the selected OS architecture in terms of lenses material, shapes, and arrangement. To characterize the OS performances for ITER applications, we use as the criterion its ability to resolve the 3.6 line/mm or a detail of 2.7 μm (this value is due to the pixels size) of the NBS1963a target.

III. OS AND IS ARCHITECTURE DESIGNS

To estimate the photometry budget of the ITER camera, an important step consists in evaluating the optical properties of the welded steel ring, especially its albedo ρ (the ratio of irradiance reflected to the irradiance received by the welded steel ring [18]), to correctly evaluate the photon flux reaching the CIS. The main outcomes of our calculations are that for the selected LED ring architecture illustrated in Fig. 1(c); the welded steel ring can be approximated as a diffusing material with an albedo $\rho = 0.23$. The goal of establishing the photometry budget is to define the required number of LEDs to have a sufficient illuminance I_{scene} in $W \cdot m^{-2}$ in order to fully exploit the CIS dynamic range while considering an OS with an aperture of F/5 that is achievable in the camera allowed volume. Calculations detailed hereafter are

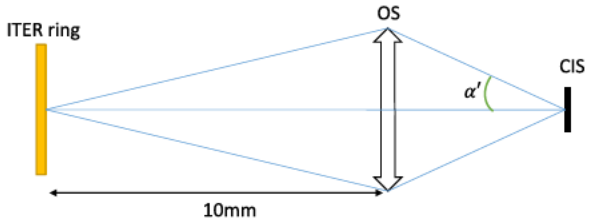

Fig. 2. Schematic of the scene, the OS, the IS, and the optic ray paths from the object to the CIS.

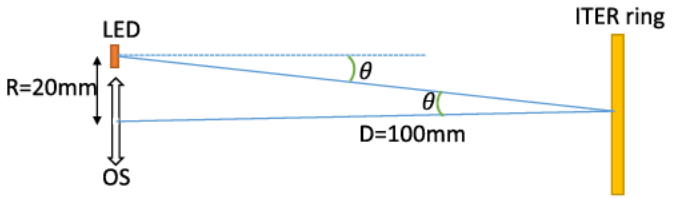

Fig. 3. Schematic of the scene, the OS, the IS, and the ray path from the LED to the OS.

based on the methodology described in [18] applied to the case described in Fig. 2.

The photon flux F_0 (in W) arriving on the central pixel of the 256 × 256 CIS demonstrator can be expressed for a diffusing material as

$$F_0 = \pi T_{\text{op}} L_{\text{scene}} A_{\text{px}} \sin^2(\alpha') \tag{4}$$

where T_{op} is the OS optical transmission in percent at the wavelength of interest, L_{scene} is the scene luminance in $\text{W} \cdot \text{sr}^{-1} \cdot \text{m}^{-2}$, A_{px} is the area of a pixel in μm^2, and α' is the aperture angle (indicated in Fig. 2). For a Lambertian scene L_{scene} is

$$L_{\text{scene}} = \frac{\rho}{\pi} I_{\text{scene}} \tag{5}$$

where ρ is the albedo of the object and I_{scene} is the irradiance of the scene due to the IS ($\text{W} \cdot \text{m}^{-2}$). From (4) and (5), the following equation can be deduced:

$$F_0 = \rho T_{\text{op}} I_{\text{scene}} A_{\text{px}} \sin^2(\alpha') \tag{6}$$

For a monochromatic source and a given quantum efficiency η, the number N of electrons generated by second in a pixel is

$$N = \eta \frac{F_0}{h\frac{c}{\lambda}} \tag{7}$$

For C_p is the pixel capacity in electrons and τ is the integration time in millisecond, from (6) and (7) the following relation is obtained:

$$N\tau = \frac{C_p}{2} \leftrightarrow \frac{\eta\lambda}{hc} \rho T_{\text{op}} I_{\text{scene}} A_{\text{px}} \sin^2(\alpha')\tau = \frac{C_p}{2} \tag{8}$$

Hence

$$C_p = I_{\text{scene}} \times 2\frac{\eta\lambda}{hc} \rho T_{\text{op}} A_{\text{px}} \sin^2(\alpha')\tau \tag{9}$$

From this, we have to calculate how many photons the LEDs have to generate to ensure that a sufficient numbers of electrons are generated in the central pixel to exploit its full dynamic. For these calculations, the LEDs are considered as punctual and Lambertian, and within a ring surrounding the OS as described in Fig. 3

From Fig. 3, we deduce $\theta = 0.20$ rad. For a Lambertian LED, its intensity I expressed in $\text{W} \cdot \text{sr}^{-1}$ is given by

$$I(\theta) = I_{\max} \cos(\theta) \tag{10}$$

The maximum of the emission is calculated from the total flux of the LED F_{tot} in W

$$\begin{aligned} F_{\text{tot}} &= \int_0^{\frac{\pi}{2}} I_{\max} \cos(\theta) \times 2\pi \times \sin(\theta) d(\theta) \\ &= \pi I_{\max} \end{aligned} \tag{11}$$

$$I_{\max} = \frac{F_{\text{tot}}}{\pi} \tag{12}$$

With (10) and with respect to the geometric considerations from Fig. 3, we can deduce

$$I_{\text{scene}} = N I_{\max} \frac{\cos^4(\theta)}{D^2} \tag{13}$$

where N is the total number of LED in the IS ring (typically 20). By including (12) and (13) in (10), we can calculate at each wavelength the number of electrons generated in the central pixel. For polychromatic systems, we must also consider the transmission coefficient of the pixel filters T_{filter}. There are three types of filter: red, green, and blue, needed to obtain RGB images. As a consequence these results will be given for each class of filter which are described in [3]

$$C_p = I_{\text{scene}}(\lambda) 2 \frac{\eta(\lambda) \times \lambda}{hc} \rho(\lambda) T_{\text{op}}(\lambda) A_{\text{px}}(\lambda) \sin^2(\alpha') \tau T_{\text{filter}(\lambda)} \tag{14}$$

In the context of our study, the IS is considered as radiation tolerant if, after irradiation, the number of photo-generated electrons (induced by the full ring lighting) during the integration time τ is higher than half the capacity of the CIS: $C_p = 10^5$electrons [3].

IV. Radiation Test Results and Discussion

A. Results on LEDs

Table III gives the emitted power measured before and after each irradiation step for each individual LEDs. Those values are obtained for a unique LED while the last column expressed if the IS still fulfills the ITER needs after 1.1 MGy.

Figs.4 and 5 show the radiation-induced changes for amber and white LEDs. The two most radiation resistant LEDs of each type are Fig. 4 W#1 and Fig. 5 A#3. These results also reveal that most of the tested LEDs are quite radiation tolerant at MGy dose. Indeed, the reduction of the luminous flux is typically lower than ~30%, except for one amber LED (~60%, Fig. 5 A#2).

Surprisingly, by comparing the two versions of W#5 and A#3 with and without the silicon lens, the lens does not seem impacted too much by γ -rays. Indeed, Fig. 6 shows that after 1.1 MGy, the spectral ratio between the total flux emitted

TABLE III

EVOLUTION OF THE LED EMISSION PROPERTIES WITH DOSE

LED	Power before irrad (W)	Power after 0.1MGy (W)	Power after 0.5MGy (W)	Power after 1.1MGy (W)	change after 1.1 MGy (%)	IS Iter*
A#1	0.07	0.09	0.07	0.04	39.12	NO
A#2	0.12	0.15	0.09	0.05	59.29	NO
A#3 with SL (Silicon Lens)	0.46	0.44	0.45	0.44	5.34	AV
A#3 no SL	0.36	0.36	0.35	0.35	3.31	**
W#1	1.73	1.73	1.67	1.65	4.54	OK
W#2	0.33	0.33	0.29	0.24	27.22	NO
W# 3	0.22	0.24	0.20	0.15	31.89	NO
W# 4	0.39	0.37	0.31	0.26	33.31	NO
W# 5 with SL	0.51	0.48	0.45	0.36	29.43	AV
W# 5 no SL	0.30	0.29	0.25	0.20	32.54	**
W# 6	0.47	0.47	0.41	0.41	12.72	AV

* This last column expresses if the IS still fulfill the ITER requirements after irradiation, considering the OS and IS degradation and no CIS quantum efficiency degradation in agreement with [3]: OK= margin > 5, AV= margin <5 and NO= below requirements.** For LEDs with removed silicon lens, as the radiation diagram is no longer known, the calculations cannot be done.

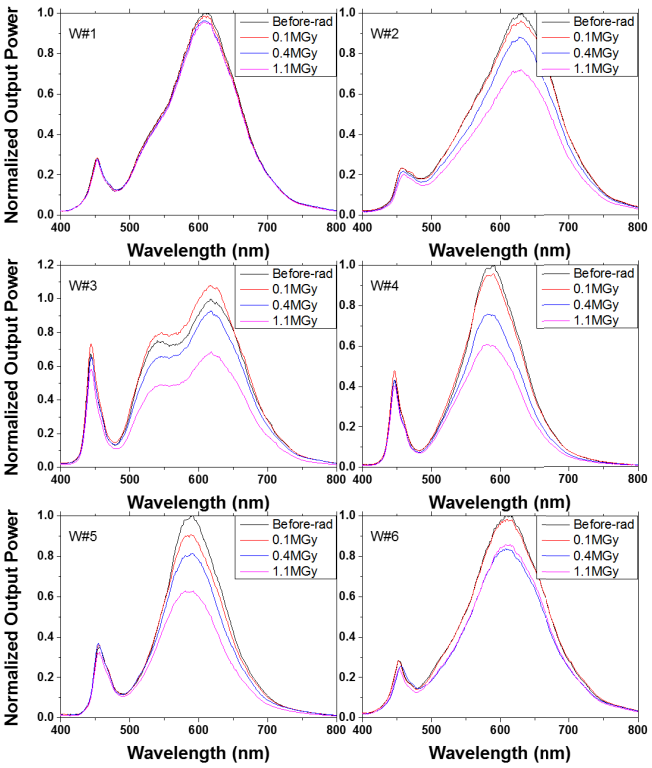

Fig. 4. White LED W#1–6 normalized spectral output powers at different doses. The normalization consists in dividing by the maximum value of the before radiation spectrum.

by the same LED with and without SL is roughly the same than before irradiation.

While Fig. 5 A#2 is a direct emitting AlInGaP LED, Fig. 5 A#3 LED is a 450 nm emitting InGaN device, which

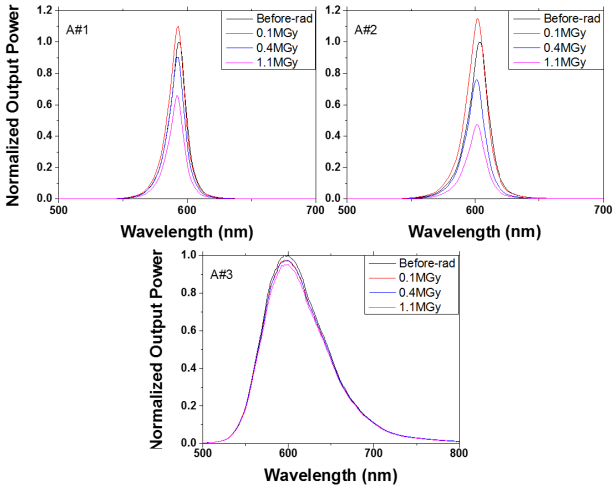

Fig. 5. Amber LED A#1–3 normalized spectral output powers at different doses. The normalization consists in dividing by the maximum value of the before radiation spectrum.

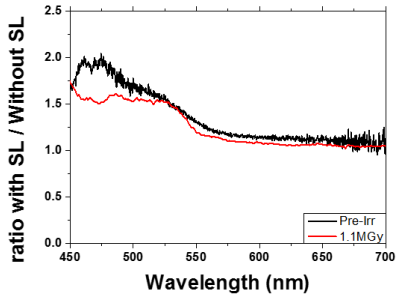

Fig. 6. Flux ratio between the same LED with and without an SL before and after irradiations for W#5.

employs a phosphor-conversion layer to convert its 450 nm emission into an "amber" spectrum around 600 nm. Our results show that Fig. 5 A#3 is less degraded (−5.34%) in the range of dose investigated than Fig. 5 A#1 (−39.12%) and Fig. 5 A#2 (−59.29%). This agrees with [19] that concluded that (In,Ga)N-based materials and devices are more radiation resistant than those exploiting (Al,Ga,In)P materials.

Different behaviors are observed for the white LEDs. Fig. 4 W#1 is almost unaffected by radiations (−4.5% after 1.1 MGy). Fig. 4 W#3 exhibits a decrease of its emission, both in the blue part of the spectrum and in the phosphor-converted region. Last case Fig. 4 W#5 shows a decrease only in the converted part of the spectrum, suggesting a degradation of the phosphor conversion. Interestingly, the most radiation tolerant device Fig. 4 W#1 is a high-power device, while all the others are mid-power LEDs. However, in the absence of more details from LED manufacturers, it is difficult to analysis in detail this discrepancy. LEDs W#3, A#1, A#2 (Figs. 3 and 4), either amber or white, also present a minor increase (+20% at best) of their emitted powers at the first dose level (0.1 MGy). To the best of our knowledge, this phenomenon has never been observed by other authors, either with gamma or other type of radiations and its origin deserves further experiments.

InGaN blue emitting LEDs are known to be affected by the phenomena of "efficiency droop," i.e., a decrease of quantum

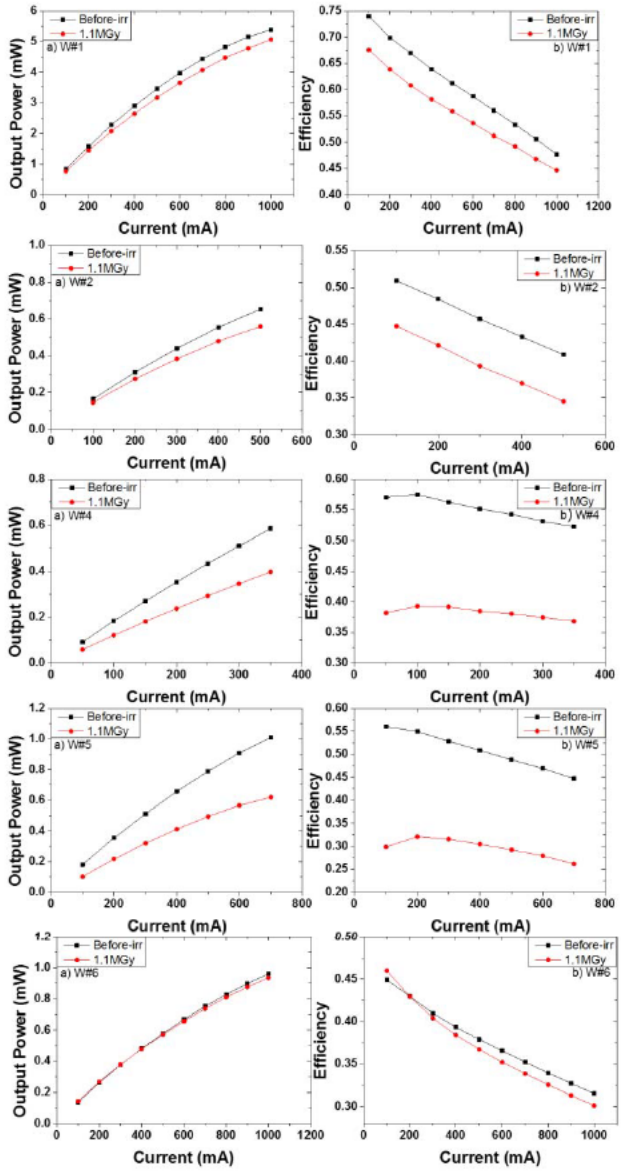

Fig. 7. Impact of radiation on the "efficiency droops" for white LEDs. (a) W# optical power versus current for white LED. (b) W# efficiency (photons emitted/electrons injected).

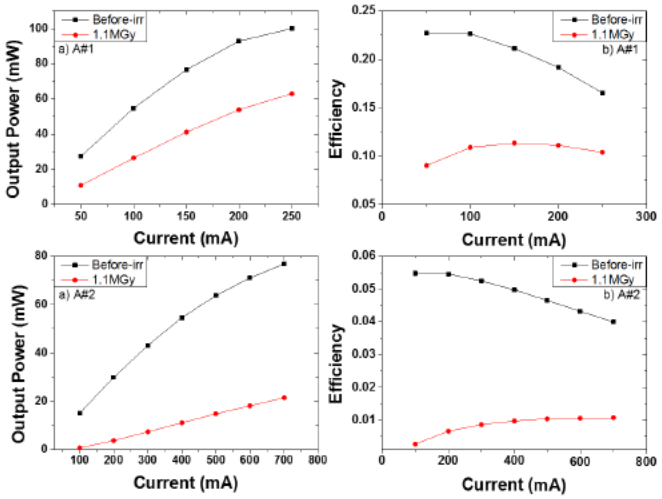

Fig. 8. Impact of radiation on the "efficiency droops" for amber LEDs. (a) A# optical power versus current for amber LED. (b) A# efficiency (photons emitted/electrons injected).

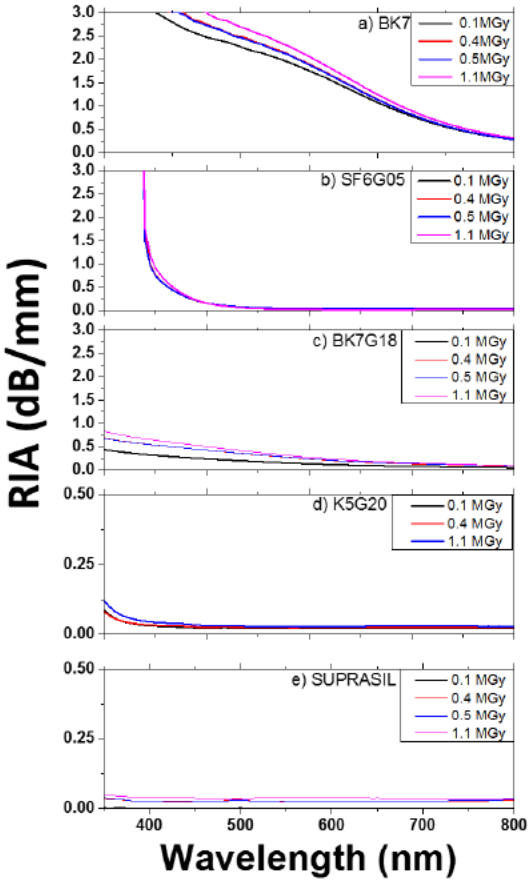

Fig. 9. RIA spectral dependence at the various doses. (a) BK7, (b) SF6G05, (c) BK7G18, (d) K5G20, and (e) SUPRASIL glasses.

efficiency at high injected current [20], attributed to Auger recombination [21]. The phenomenon of efficiency droop is as expected present in all tested samples (see Figs.7 and 8), since the efficiency (radiation flux divided by electrical power) tends to decrease when increasing the drive current. However, if the irradiation indeed decreases the output power, it does not significantly affect the slope of the efficiency versus current curve, suggesting that the efficiency droop remains unaltered.

Regarding AlInGaP amber devices (Fig. 8), a droop of efficiency is also observed for the not irradiated device, however, less pronounced than in InGaN devices. In the literature, this phenomenon is usually not observed for AlInGaP, except in [22], where it was also detected, but only at low temperature. However, after irradiation, contrary to the case of InGaN, the droop of efficiency in AlInGaP amber devices almost disappears. One possible explanation for this unexpected observation is that recombination may be so enhanced by radiation that the level of electrons and holes concentrations required for Auger recombination is no longer achieved, removing efficiency droop. The overall low level of efficiency and strong impact of radiation on it for AlInGaP amber devices are in favor of this hypothesis.

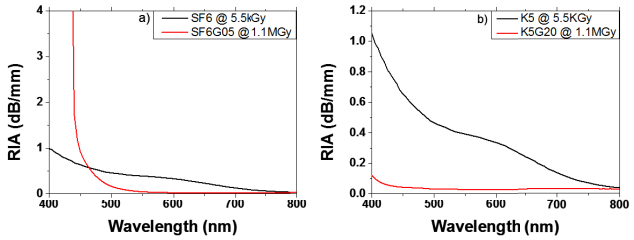

Fig. 10. Comparison between RIA of non-RH glass and there RH version. (a) SF6 and SF6G05. (b) K5 and K5G20. For SF6 and K5 RIA were calculated from [12].

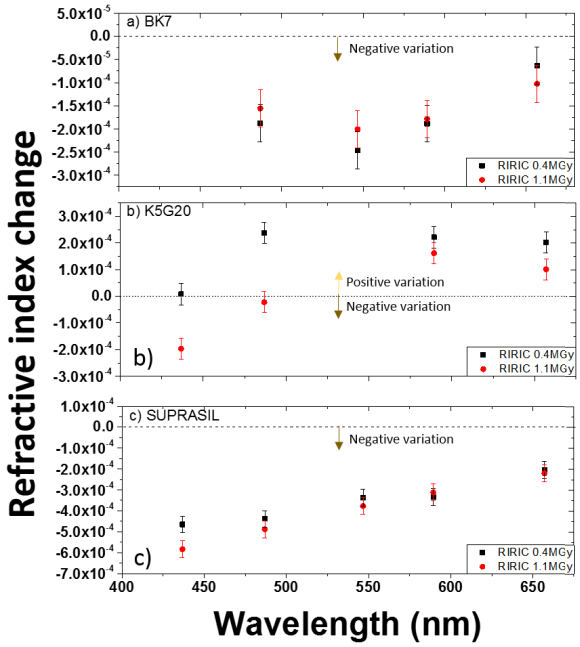

Fig. 11. RIRIC spectral dependence at the various doses. (a) BK7, (b) K5G20, and (c) SUPRASIL glasses.

B. Results on Bulk Glasses

Fig. 9 illustrates the RIA spectral dependences at the various doses for BK7, SF6G05, BK7G18, K5G20, and SUPRASIL glass, respectively. The RIA above 500 nm remains limited for SCHOTT Ltd RH glasses (Fig. 9(b)–(d)) and very low for the pure silica glass (Fig. 9(e)), whereas it is larger for BK7. To better highlight the good resistance of these glasses in terms of permanent damages at RT, we compared RIA of SF6G05 and K5G20 glasses to their non-RH counterparts (SF6 and K5), in Fig. 10, exposed to low-radiation doses of a few kGy [12].

Fig. 10 shows that the Ce doping is efficient to decrease for all these glasses even if it seems less efficient to improve the SF6G05 glass under 500 nm. For a monochromatic system operating around 600 nm, the RIA should be acceptable for the various OS designs, whereas for color systems, a more in-depth study has to be conducted to see how radiations will affect the colorimetry of the recorded images, especially at lower wavelengths where the photometry budget possesses the smallest margins and the radiation effects are the larger.

We measured also the RIRIC after the second (up to 0.4 MGy) and the third (up to 1.1 MGy) irradiation run.

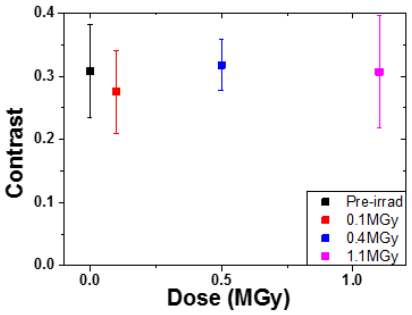

Fig. 12. Evolution of the contrast at various doses. Error bars are representing the dispersion originating from the measurements repetitions. Squares mark the median value.

Obtained results are given in Fig. 11(a)–(c) for the two RH glasses exhibiting RIRIC higher than 2×10^{-4}. For the SUPRASIL glass, the RIRIC is larger than 5×10^{-4}.

We selected our wavelengths to be able to calculate the Abbe number that is a measure of the refractive index variation versus wavelength and use it for future simulations. For the BK7 there is nearly no more RIRIC increase after a total dose between 0.4 and 1.1 MGy, as observed for the RIA that tends to saturation at larger doses [23]. For K5G20, the RIRIC modification between 0.4 and 1.1 MGy appears more important. For the SUPRASIL with really a low RIA, this modification of the refractive index may rather be attributed to a slight modification of the glass density rather than to absorption. RIRIC is usually considered as the result of two modifications: density change [24] and RIA [15] (through Kramer–Krönig relation). These two modifications are linked and there are no consensus about the leading one in our dose range, in both cases refractive-index modification may be positive or negative [25] and [26]. To be able to give a full understanding of the RIRIC, it will be necessary to measure the density change and the RIA in the UV part of the spectrum with a great accuracy. For the cerium-doped glasses such measurement is prevented by the cerium-induced attenuation below 500 nm and for the BK7 case, the numerous impurity prevents also this measurement. Gusarov *et al.* [15] attribute the existence of a positive variation of refractive index to a side effect of Ce. Average composition of BK7 and other none pure silica glasses are globally known [27]–[30] but remains quite complex to allow an easy identification of the point defects responsible for the RIA and RIRIC. In term of OS design, the RIRIC effects have to be considered. To make the OS tolerant by design, it is possible to use the simulation tools [31] to design an OS architecture more robust against RIRIC of its lenses. Glass with a high RIA could not be used in an radiation tolerant OS but for low RIA glasses with known RIRIC values before starting the conception phase it will be possible to enhance the design quality, even maybe compensate the RIRIC of the lenses made with different materials.

C. Results on the Illumination System

The whole photometry budget for the camera has been done again after irradiation by including in our calculations,

the observed degradation for the IS (LED output power decrease) and OS (spectral dependence of RIA). For the CIS, as shown in [3], we could consider as a first approximation that the filter transmission and the quantum efficiency remain unaffected at MGy dose. From this analysis, three cases are considered for the various IS designs and their ranking is done in the last column of Table III. For all designs labeled as "OK," the IS still delivers after irradiation more than 5 times the number of photons required to exploit the CIS dynamic. These designs are then very robust, giving sufficient margins to have confidence in their potential for ITER applications. Furthermore, it could be possible to monitor the LEDs at an intermediate current, reducing the thermal effects issue and offering the capability to increase the photon flux if needed to compensate RIA of the OS. For the IS labeled as "AV," the ratio is below 5, with less margins for the camera conception, but sufficient margins to be confident on their functionalities. For the IS noted as "NO," the ratio is below 2, for some LEDs, below 1, these IS cannot be used for the ITER applications without increasing the number of LEDs in the IS.

D. Result on the Optical System

To characterize the manufactured OS (Fig. 1(b)), contrast measurements have been done and typical results obtained for the monochrome OS are illustrated in Fig. 1(b). As it can be seen, the contrast does not significantly evolve with the dose. For the developed miniaturized OS, the commercial test benches cannot be used, a homemade setup was elaborated at the Laboratoire Hubert Curien, the errors bars are obtained by repeating more than 20 times the contrast measurements from scratch.

These experimental results agree with simulations of the OS contrast done with the OpticStudio code and considering the RIRIC changes measured on the glasses used for the OS. It is shown that for this OS design; the measured RIRIC are not sufficient to degrade significantly the OS modular transfer function.

V. Conclusion

This paper summarizes the main outcomes of the FURHIS project aiming to develop radiation-hardened OS and ISs that could be used as subsystems of MGy radiation-hardened color or monochrome cameras for ITER remote handling operations. Presented results (and those presented in [3] for the CIS) demonstrate that commercially available LEDs and bulk glass materials exist that are intrinsically tolerant to radiation permanent damages. Using the appropriate technologies for the materials and component, we showed that IS and OS with the performances needed by ITER can be conceived and the tests of these system demonstrators demonstrate that these performances remain acceptable even after irradiation at MGy dose levels. Furthermore, it is possible to select IS architectures allowing to provide enough margins in terms of output power to reduce thermal management issues and eventually compensate for the RIA of the optical lenses. In terms of perspectives, a fully integrated camera prototype will be developed in the framework of a future project, exploiting the knowledge acquired during the FURHIS project.

DISCLAIMER

The views expressed in this publication are the sole responsibility of the authors and do not necessarily reflect those of the ITER Organization or Fusion for Energy. Neither Fusion for Energy nor any person acting on behalf of Fusion for Energy is responsible for the use which might be made of the information in this publication.

References

[1] European Fusion Development Agreement. (2006). *The ITER Project*. [Online]. Available: https://web.archive.org/web/20060824071609/http://www.efda.org/the_iter_project/index.htm

[2] S. Girard, "Multi-MGy radiation hardened camera for nuclear facilities," presented at the Advancements Nucl. Instrum. Meas. Methods Appl. (ANIMMA), Lisbon, Portugal, Apr. 2015.

[3] V. Goiffon *et al.*, "Total ionizing dose effects on a radiation hardened CMOS image sensor demonstrator for ITER remote handling," *IEEE Trans. Nucl. Sci.*, to be published, doi: 10.1109/TNS.2017.2765481.

[4] D. Doyle, "Radiation hardness of optical materiel," presented at the 3rd Eur. Jupiter Syst. Mission Instrum. Workshop (ESA ESTEC), Noordwijk, The Netherlands, Jan. 2010.

[5] S. J. Pearton, R. Deist, F. Ren, L. Liu, A. Y. Polyakov, and J. Kim, "Review of radiation damage in GaN-based materials and devices," *J. Vac. Sci. Technol. Vac. Surf. Films*, vol. 31, no. 5, pp. 050801-1–050801-15, Sep. 2013.

[6] R. Khanna, S. Y. Han, S. J. Pearton, D. Schoenfeld, W. V. Schoenfeld, and F. Ren, "High dose Co-60 gamma irradiation of InGaN quantum well light-emitting diodes," *Appl. Phys. Lett.*, vol. 87, no. 21, pp. 212107-1–212107-3, Nov. 2005.

[7] A. H. Johnston, "Radiation damage of electronic and optoelectronic devices in space," in *Proc. 4th Int. Workshop Radiat. Effects Semiconductor Devices Space Appl.*, 2000, pp. 1–9. [Online]. Available: http://nepp.nasa.gov/docuploads/D41D389D-04D4-4710-BBCFF24F4529B3B3/Dmg_Space-00.pdf

[8] G. A. Umana-Membreno *et al.*, "^{60}Co gamma-irradiation-induced defects in n-GaN," *Appl. Phys. Lett.*, vol. 80, no. 23, pp. 4354–4356, Jun. 2002.

[9] K. N. Orlova, A. V. Gradoboev, and I. A. Asanov, "Gamma degradation of light-emitting diodes based on heterostructures AlGaInP," in *Proc. 7th Int. Forum Strategic Technol. (IFOST)*, Sep. 2012, pp. 201–204.

[10] T. Takeuchi *et al.*, "Development of radiation-resistant in-water wireless transmission system using light emitting diodes and photo diodes," *IEEE Trans. Nucl. Sci.*, vol. 63, no. 5, pp. 2698–2702, Oct. 2016.

[11] R. Mueller-Mach *et al.*, "All-nitride monochromatic amber-emitting phosphor-converted light-emitting diodes," *Phys. Status Solidi-Rapid Res. Lett.*, vol. 3, nos. 7–8, pp. 215–217, Oct. 2009.

[12] I. Manolis *et al.*, "The ESA RADGLASS activity: A radiation study of non rad-hard glasses," *Proc. SPIE*, vol. 9639, pp. 96391N-1–96391N-15, Oct. 2015.

[13] *Technical Note: Radiation Resistant Optical Glasses*, Schott Ltd., London, U.K., Feb. 2007.

[14] S. Baccaro, A. Cemmi, I. Di Sarcina, and F. Menchini, "Gamma rays effects on the optical properties of cerium-doped glasses," *Int. J. Appl. Glass Sci.*, vol. 6, no. 3, pp. 295–301, Sep. 2015.

[15] A. I. Gusarov *et al.*, "Refractive-index changes caused by proton radiation in silicate optical glasses," *Appl. Opt.*, vol. 41, no. 4, pp. 678–684, 2002.

[16] A. F. Fernandez *et al.*, "SCK·CEN gamma irradiation facilities for radiation tolerance assessment," in *Proc. IEEE Radiat. Effects Data Workshop*, Jul. 2002, pp. 171–176.

[17] M. Hébert, R. D. Hersch, and P. Emmel, "Fundamentals of optics and radiometry for color reproduction," in *Handbook of Digital Imaging*, M. Kriss, Ed. Chichester, U.K.: Wiley, 2014, pp. 1–57.

[18] J.-L. Meyzonnette and T. Lépine, *Bases de Radiométrie Optique*. Toulouse, France: Cépaduès Éd, 1999.

[19] A. Ionascut-Nedelcescu, C. Carlone, A. Houdayer, H. J. von Bardeleben, J.-L. Cantin, and S. Raymond, "Radiation hardness of gallium nitride," *IEEE Trans. Nucl. Sci.*, vol. 49, no. 6, pp. 2733–2738, Dec. 2002.

[20] M.-H. Kim *et al.*, "Origin of efficiency droop in GaN-based light-emitting diodes," *Appl. Phys. Lett.*, vol. 91, no. 18, pp. 183507-1–183507-3, Oct. 2007.

[21] Q. Dai *et al.*, "On the symmetry of efficiency-versus-carrier-concentration curves in GaInN/GaN light-emitting diodes and relation to droop-causing mechanisms," *Appl. Phys. Lett.*, vol. 98, no. 3, pp. 033506-1–033506-3, 2011.

[22] J. Cho, E. F. Schubert, and J. K. Kim, "Efficiency droop in light-emitting diodes: Challenges and countermeasures," *Laser Photon. Rev.*, vol. 7, no. 3, pp. 408–421, May 2013.

[23] G. H. Meeten, "Refractive index errors in the critical-angle and the Brewster-angle methods applied to absorbing and heterogeneous materials," *Meas. Sci. Technol.*, vol. 8, no. 7, pp. 728–733, 1997.

[24] B. Poumellec, P. Niay, M. Douay, and J. F. Bayon, "The UV-induced refractive index grating in Ge:SiO_2 preforms: Additional CW experiments and the macroscopic origin of the change in index," *J. Phys. D, Appl. Phys.*, vol. 29, no. 7, pp. 1842–1856, 1996.

[25] J. A. Ruller and E. J. Friebele, "The effect of gamma-irradiation on the density of various types of silica," *J. Non-Cryst. Solids*, vol. 136, nos. 1–2, pp. 163–172, Dec. 1991.

[26] A. Bishay, "Radiation induced color centers in multicomponent glasses," *J. Non-Cryst. Solids*, vol. 3, no. 1, pp. 54–114, Jan. 1970.

[27] *N-BK7 Technical Safety Information*, Schott Ltd., London, U.K., Mar. 2015.

[28] *SF6G05 Technical Safety Information*, Schott Ltd., London, U.K., Mar. 2015.

[29] *BK7G18 Technical Safety Information*, Schott Ltd., London, U.K., Mar. 2015.

[30] *K5G20 Technical Safety Information*, Schott Ltd., London, U.K., Mar. 2015.

[31] C. Muller *et al.*, "Extrapolated degradation of optical systems at MGy levels due to radiation-induced refractive index change," *IEEE Trans. Nucl. Sci.*, to be published.